RESEARCH ARTICLE | JANUARY 02 2025

Multihyperuniformity in high-entropy MXenes

Yu Liu ; Mohan Chen

Appl. Phys. Lett. 126, 013101 (2025)
https://doi.org/10.1063/5.0246719

Applied Physics Letters ARTICLE pubs.aip.org/aip/apl

Multihyperuniformity in high-entropy MXenes

Cite as: Appl. Phys. Lett. **126**, 013101 (2025); doi: 10.1063/5.0246719
Submitted: 4 November 2024 · Accepted: 12 December 2024 ·
Published Online: 2 January 2025

View Online Export Citation CrossMark

Yu Liu[1,2] and Mohan Chen[1,2,a)]

AFFILIATIONS

[1]HEDPS, CAPT, College of Engineering and School of Physics, Peking University, Beijing 100871, People's Republic of China
[2]AI for Science Institute, Beijing 100080, People's Republic of China

[a)]Author to whom correspondence should be addressed: mohanchen@pku.edu.cn

ABSTRACT

MXenes are a large family of two-dimensional transition metal carbides and nitrides that possess excellent electrical conductivity, high volumetric capacitance, great mechanical properties, and hydrophilicity. In this work, we generalize the concept of multihyperuniformity, an exotic state that can exist in a disordered multi-component system, to MXenes. Disordered hyperuniform systems possess an isotropic local structure that lacks traditional translational and orientational order, yet they completely suppress infinite-wavelength density fluctuations as in perfect crystals and, in this sense, possess a hidden long-range order. In particular, we evaluate the static structure factor of the individual components present in the high-entropy (HE) MXene experimental sample TiVCMoCr based on high-resolution scanning electron microscope imaging data, which suggests that this HE MXene system is at least effectively multihyperuniform (MH). We then devise a packing algorithm to generate MH models of HE MXene systems. The MH HE MXenes are predicted to be energetically more stable compared to the prevailing (quasi)random models of the HE MXenes due to the hidden long-range order. Moreover, the MH structure exhibits a distinctly smaller lattice distortion, which has a vital effect on the electronic properties of HE MXenes, such as the density of states and charge distribution. This systematic study of HE MXenes strengthens our fundamental understanding of these systems and suggests possible exotic physical properties, as endowed by the multihyperuniformity.

MXenes, a family of two-dimensional (2D) metal carbides and nitrides with a general formula of $M_{n+1}X_nT_x$ (n = 1-4), are structured with two or more layers of transition metal (M) atoms arranged in a honeycomb-like 2D lattice, interspersed with carbon and/or nitrogen (X) layers occupying the octahedral sites between adjacent transition metal layers.[1,2] Terminal groups of MXenes such as −OH, −O, and −F, commonly denoted as T_x, are tunable during etching A-layer from the layered hexagonal MAX phases,[3,4] where A is an element mainly from groups 13–16 of the periodic table. Owing to the unique 2D structure, MXenes exhibit excellent electrical conductivity,[5] high volumetric capacitance,[6] great mechanical properties,[7] and hydrophilicity.[8] Thanks to their outstanding properties, MXenes have been extensively investigated for potential applications in various fields, such as batteries,[9–15] electromagnetic interference shielding,[16,17] electrocatalysis,[18–20] supercapacitors,[21,22] and so on.

High-entropy materials (HEMs) are a class of materials composed of mixtures of equal or relatively large proportions of multiple principal elements.[23,24] Highly diversified structures enable HEMs to exhibit unexpected mechanical, physical, and chemical properties, offering great promise for applications in mechanics, energy storage, and conversion.[25–28] In 2021, the high-entropy (HE) strategy was extended into the MXene design space, further enhancing its tunability.[29] HE MXenes have great potential for energy storage and conversion due to their vast configurational space.[30–32] However, only a few HE MXenes have been synthesized successfully due to the difficulties in preparation. The distribution of transition metal atoms in HE MXenes remains elusive. In terms of theoretical calculations of HE MXenes,[33] the dominant models employed are random mixture and special quasirandom structure (SQS) models.[34,35] However, we notice that the clustering of atoms of the same type is suppressed as displayed in elemental mapping images of recent experimental studies.[31,36,37] Given that atoms prefer specific neighboring configurations, which are not captured by random mixture and SQS models, we anticipate that when an observation window is randomly shifted throughout the system, the count of atoms of a particular element within that window would exhibit little fluctuations, especially for larger window sizes.

Hyperuniformity[38] is a special long-range order characterized by an ordered metric based on particle number variance $\sigma_N^2(R)$ in a spherical observation window, which vanishes when normalized by the observation window volume (scales as $\sim R^d$ in d-dimensional Euclidean space) in the infinite-window limit, i.e.,

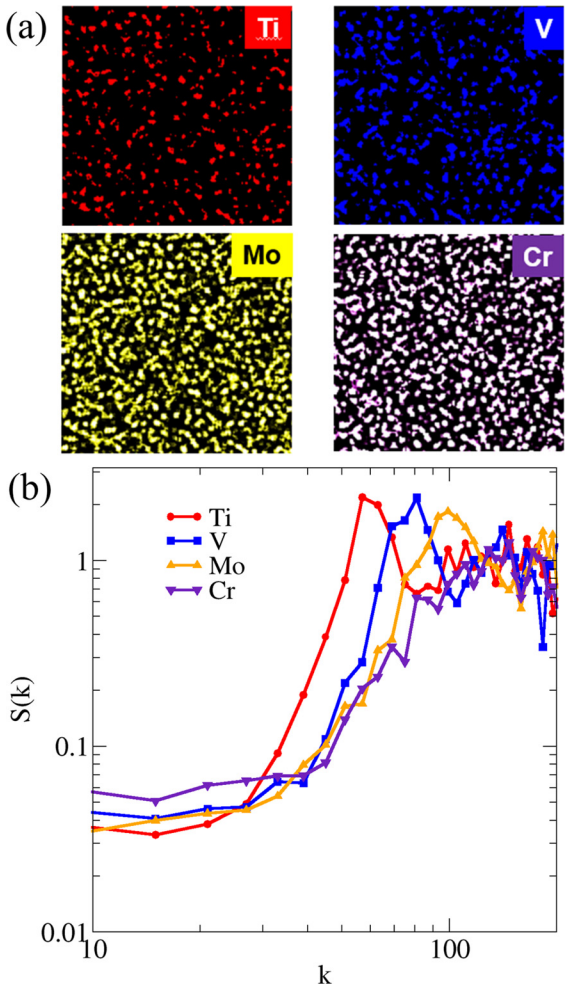

FIG. 1. (a) SEM images of the TiVCMoCr HE MXene sample[36] showing the distribution of transition metal atoms, (b) the associated static structure factor $S(k)$. The linear size of the box is $L = 20$ nm. The unit of the wavenumber is 0.1 nm^{-1}. The SEM images are reproduced with permission from He *et al.*, Adv. Mater. **35**, 2211432 (2023). Copyright 2023 Wiley-VCH GmbH.[36]

$$\lim_{r\to\infty} \sigma_N^2(R)/R^d = 0. \tag{1}$$

Hyperuniformity is equivalently manifested as the vanishing static structure factor in the infinite-wavelength (or zero-wavenumber) limit, i.e., $\lim_{k\to 0} S(k) = 0$, where k is the wavenumber. The small-k scaling behavior of $S(k) \sim k^\alpha$ determines the large-R asymptotic behavior of $\sigma_N^2(R)$, based on which all hyperuniform systems, disordered or not, can be categorized into three classes: $\sigma_N^2(R) \sim R^{d-1}$ for $\alpha > 1$ (class I); $\sigma_N^2(R) \sim R^{d-1}\ln(R)$ for $\alpha = 1$ (class II); and $\sigma_N^2(R) \sim R^{d-\alpha}$ for $0 < \alpha < 1$ (class III).[39] Consequently, hyperuniform systems encompass all crystals and quasicrystals.[38,39] Crystals belong to a special subset of class-I hyperuniform systems and possess a zero structure factor for a range of wavenumbers starting from the origin, i.e., $S(k) = 0$ for $k < K^*$ (excluding the forward scattering), which are referred to as stealthy hyperuniform systems. Disordered hyperuniform states have been observed across a broad range of equilibrium and nonequilibrium physical and biological systems and seem to confer unique desirable properties.[38–63]

Multihyperuniformity is an exotic hyperuniform state that can exist in a multi-component system, in which each component is individually hyperuniform, and consequently, the entire system is overall hyperuniform. To date, two examples of multihyperuniform (MH) systems have been reported, including the distribution of photoreceptor cones in avian retina[42] and high-entropy alloys (HEA).[64] The emergence of multihyperuniformity in such systems is typically related to certain effective mutual "exclusion effects" among the particles of the same species. For example, in the case of avian photoreceptors, once a cell's phenotype is determined, an inhibition factor is released to suppress the formation of neighboring cells of the same type.[42] Similarly, enthalpy minimization favors a heterogeneous arrangement of neighboring atoms in HEAs, in the case that atoms of the same type tend to repel each other while attracting atoms of different types. Due to the similarity of HEAs and HE MXenes, it is natural to ask the question: *Can HE MXenes in such case also be MH?*

In this work, we present a comprehensive study of multihyperuniformity in HE MXenes. We first carry out a detailed analysis of high-resolution scanning electron microscope (SEM) images via evaluating the static structure factor of the individual components present in the HE MXene experimental sample TiVCMoCr,[36] which suggests this HE MXene system is at least effectively MH (i.e., that the individual transition metal atomic species tend to distribute hyperuniformly). Motivated by this observation, we generalize a multi-scale packing algorithm[42] to generate MH structural models for HE MXenes. Using the HE MXene $(TiVZrMo)_2C$ as an example, we predict that the MH model results in a more energetically stable state compared to the commonly used random mixture configurations. The hidden long-range order in the MH models also leads to a smaller deviation from Vegard's law[65] and lower lattice distortion, which affects the electronic properties of HE MXenes.

We first employ the image processing method proposed by Jiao *et al.*[66] to analyze the SEM images of the as-prepared $TiVCrMoC_3$ HE MXene[36] to detect the hidden hyperuniformity within the system. As shown in Fig. 1(a), atoms of different types (shown as different colored dots) were identified, and their center positions were extracted and converted to a point configuration. For a single point configuration with N particles at positions $\mathbf{r}^N = (\mathbf{r}_1, \ldots, \mathbf{r}_N)$ with periodic boundaries within an orthogonal fundamental cell, the static structure factor $S(\mathbf{k})$ is given by

$$S(\mathbf{k}) = \frac{\left|\sum_{j=1}^{N} \exp(-i\mathbf{k}\cdot\mathbf{r}_j)\right|^2}{N}, \tag{2}$$

which is used to compute $S(\mathbf{k})$ directly from the point configurations associated with the atom centers derived from both experiments and simulations. Figure 1(b) shows $S(k)$ for all different types of atoms, which indicates a weak power-law behavior $S(k) \sim k^\alpha$ as $k \to 0$, where the hyperuniformity exponent $\alpha \in (0, 0.08)$ for different atomic species. An extrapolation analysis indicates the hyperuniformity index $H = S(k \to 0)/S_{peak} \approx 10^{-2}$, suggesting the HE MXenes system is at least effectively hyperuniform. We note that the SEM images may contain a curved portion of the samples, which might have degraded the degree of hyperuniformity based

on the image analysis, and the original sample might possess an even higher degree of hyperuniformity.

The study of monolayer HE MXenes is still in its early stages, with only a few studies reported so far.[67] Given the limited number of reports on HE 2D MXenes, obtaining a suitable sample with high-resolution images is challenging. To date, the as-prepared $TiVCrMoC_3$ HE MXene[36] is the most suitable for statistical analysis within the accessible experimental data. However, we note that this sample consists of four transition metal layers and three carbon layers, as well as terminal groups. Additionally, the presence of the antiferromagnetic atom Cr adds complexity to the simulation. For simplicity, we construct a three-layer HE MXene, $(TiVZrMo)_2C$, without terminal groups as the simulated system to investigate multihyperuniformity in HE MXenes using the multi-scale packing algorithm[42] described in the supplementary material. In addition, we do not construct SQS models as explained in the supplementary material. Figure 2(b) shows $S(k)$ of the simulated MH systems with equal molar fractions for all four transition metal species, possessing $\alpha \approx 1.02$ and $S(k=0) \approx 10^{-6}$. We note that since the four transition metal species are equal molar and, thus, equivalent in the configurations, we expect their $S(k)$'s are also statistically equivalent. It can be seen that the simulated systems clearly exhibit a higher degree of hyperuniformity compared to the raw image analysis. Possible reasons for this discrepancy include limited resolution of the SEM images, curvatures within the material sample, as well as the presence of defects in the sample. In contrast, the random structure shown in Fig. 2(a) exhibits an almost constant structure factor, which significantly differs from the raw image analysis.

To further validate the energetic stability of the MH HE MXenes, we compute the total energy of the MH and random structures via density functional theory (DFT)[68,69] calculations. All DFT calculations are performed using the Atomic-orbital Based *Ab-initio* Computation at UStc (ABACUS) v3.5.1 package,[70,71] which is capable of handling large systems.[57,72–74] The computational details can be found in the supplementary material. As shown in Table I, the MH structure exhibits a total energy per atom that is 8.1 meV lower than that of its random counterpart, indicating a higher degree of energetic stability in the MH HE MXene compared to the random configuration, which strongly suggests the existence of a hidden long-range order in HE MXenes. Additionally, as shown in the supplementary material, we perform DFT calculations on various independently generated MH and random structures, observing negligible variations among them. Thus, our subsequent analysis focuses on the representative MH and random structures in Fig. 2(a).

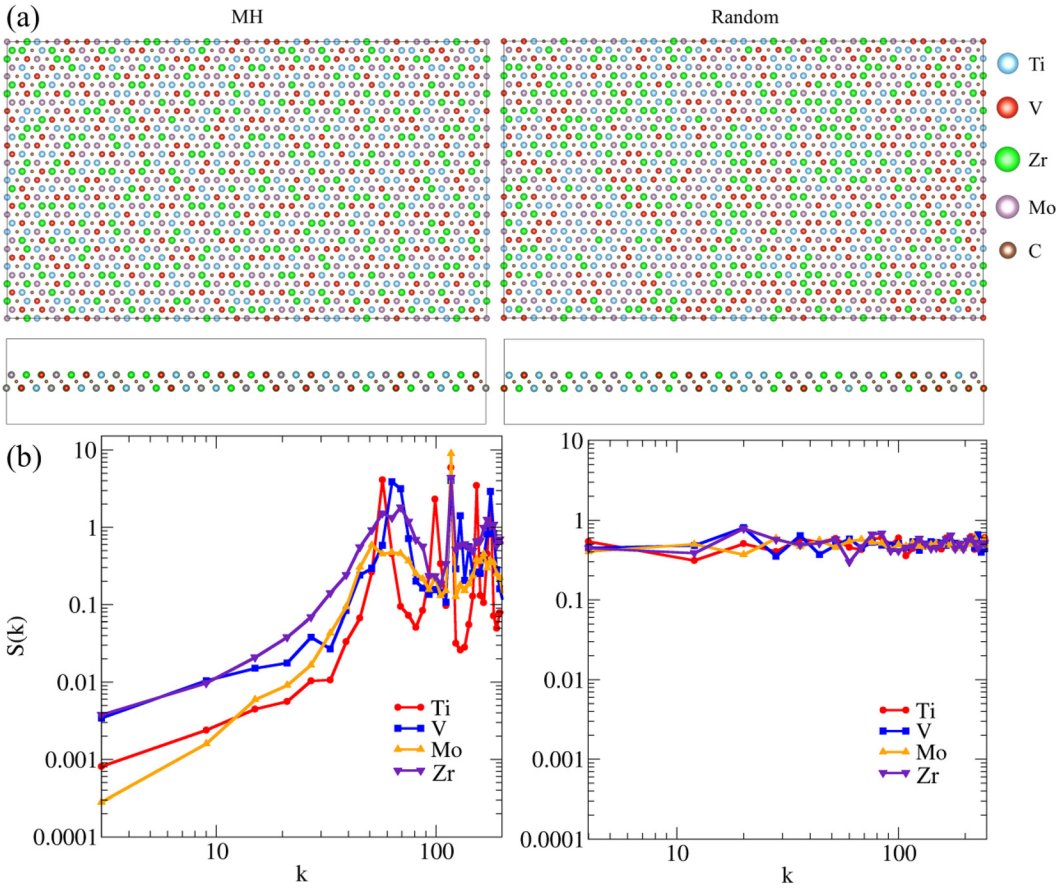

FIG. 2. (a) Top views, side views, and (b) static structure factors $S(k)$ of the representative MH model (left) and random structure (right) of $(TiVZrMo)_2C$ HE MXenes containing 1536 atoms in total. The unit of the wavenumber is 0.1 nm^{-1}.

TABLE I. The total energy per atom E, width d, and distortion parameter Δh of representative MH and random structures of $(TiVZrMo)_2C$ HE MXenes optimized via DFT calculations by ABACUS. The width d depicts the distance between the center of the two transition metal layers. The distortion parameter Δh is defined to be the average width of the transition metal layers.

Structures	MH	Random
E (eV/atom)	−1161.4439	−1161.4358
d (Å)	2.319	2.310
Δh (Å)	0.613	1.286

We predict that MH structures with suppressed composition fluctuations exhibit a smaller deviation from Vegard's law than random structures. As displayed in Table I, the width d (i.e., the distance between the center of the two transition metal layers) of the MH and random structures of $(TiVZrMo)_2C$ HE MXenes optimized by DFT calculations is 2.319 and 2.310 Å, respectively. According to Vegard's law, the width d of an equimolar $(TiVZrMo)_2C$ HE MXene is predicted to be 2.327 Å, the weighted average width d of pure Ti_2C (2.309 Å), V_2C (2.175 Å), Zr_2C (2.543 Å), and Mo_2C (2.280 Å) MXenes. The results indeed validate our assumption that the MH structure exhibits a smaller deviation from Vegard's law and reflects the nearly ideal mixing of multiple transition metal elements in the HE MXenes.

In single transition metal MXenes, the transition metal atoms within the same layer are positioned on a parallel horizontal plane. However, owing to the disparities in atomic sizes and the intricate interplay among multiple transition metal elements in HE MXenes, these transition metal atoms exhibit a certain degree of displacement, leading to the loss of planarity in the atomic layers. Thus, we also evaluate the lattice distortion via a metric Δh, which is defined to be the average width of the transition metal layers. We find that the distortion parameter Δh of the MH structure (0.613 Å) is much less than that of the random structure (1.286 Å). The MH configuration exhibits a distinctly smaller lattice distortion, resulting in a more energetically stable state compared to its random counterparts. The enhanced stability of the MH system can be attributed to the suppressed composition fluctuations. In terms of the relationship between lattice distortion and energy storage applications, previous studies suggested that the strong strains induced by lattice distortion enable to effectively guide the nucleation and uniform growth of dendrite-free lithium on HE MXene layers, delivering a stable cycling performance and good deep stripping-plating levels.[75] Such a vital correlation emphasizes the importance of structural modeling methods in theoretical simulations. In this respect, the more stable MH structures predict more accurate computational results than the random structures for HE MXenes.

We also investigate the effect of MH long-range order on the electronic structure of the $(TiVZrMo)_2C$ HE MXenes. The density of states (DOS) and projected density of states (PDOS) of representative MH and random structures of $(TiVZrMo)_2C$ HE MXenes are plotted in Fig. 3. Notably, we observe that the gap, present at approximately −3 eV below the Fermi level in the DOS of the MH configuration, is absent in that of the random structure. Prior research works indicate that mechanical strain influences the electronic properties of graphene, leading to the opening and closing of bandgaps,[76,77] which is similar to our findings in the context of HE MXenes. In the random structure for

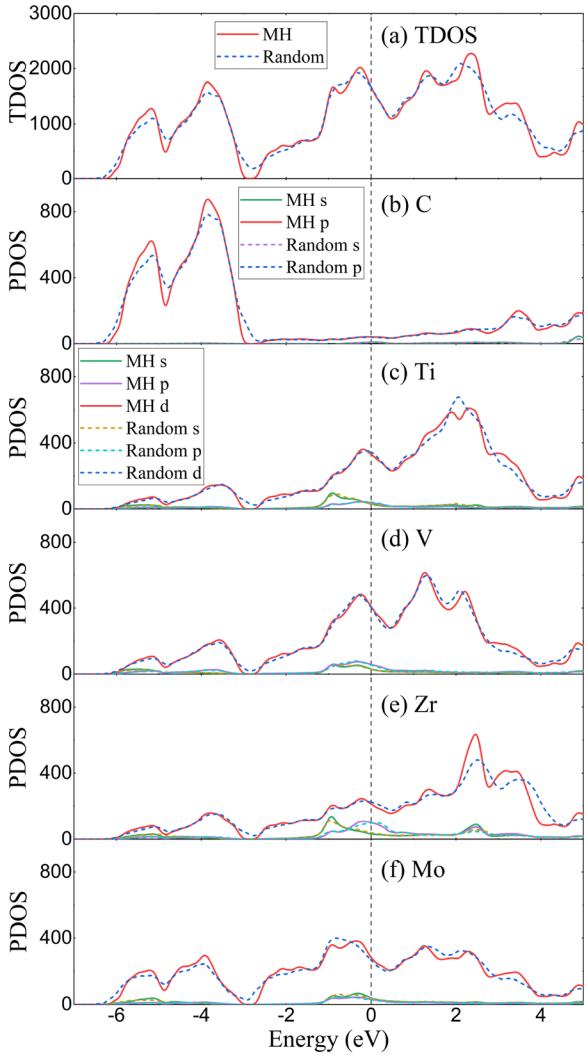

FIG. 3. Density of states (top panel) and projected density of states (bottom panel) of representative MH and random structures of $(TiVZrMo)_2C$ HE MXenes. The Fermi level is shifted to 0 eV.

the $(TiVZrMo)_2C$ HE MXene, large lattice distortion arises from the local atom clustering of the same atomic species, which is suppressed due to the presence of long-range order inherent to the MH model. As an intuitive manifestation, we plot the charge density difference $\Delta\rho$ between the MH and random structures of $(TiVZrMo)_2C$ HE MXenes. As shown in Fig. 4, we observe that the distribution of charge density in the random structure is not uniform compared to that of the MH structure due to the local atom clustering of the same atomic species. According to the PDOS panel in Fig. 3, DOS around the Fermi level arises mainly from the d orbitals of the transition metal atoms, suggesting that the electric conductivity is mainly attributed to the d electrons in the outer region. In addition, we note that the d orbitals of transition metal atoms and the p orbitals of carbon atoms overlap from −6 to −3 eV below the Fermi level, indicating strong hybridization between them.

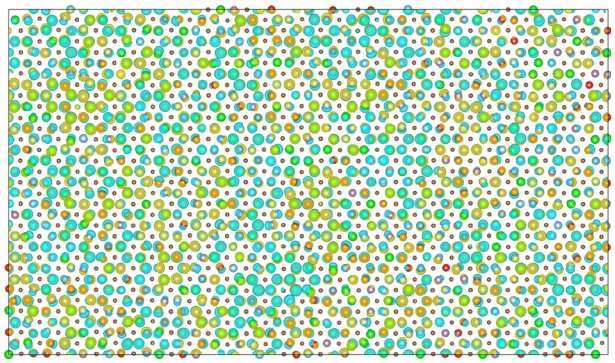

FIG. 4. The charge density difference $\Delta\rho$ between the MH and random structures of $(TiVZrMo)_2C$ HE MXenes. The isosurface value is set to 0.15.

Finally, we investigate the charge transfer of multiple atomic species in the MH and random structures of $(TiVZrMo)_2C$ HE MXenes using the Bader charge analysis method.[78–80] As shown in Table II, carbon atoms gain valence electrons, whereas all transition metal atoms lose valence electrons due to the much stronger electronegativity of carbon atoms than transition metals. The transition metal atoms mainly donate d electrons, which bond with p electrons of C atoms, thus causing the strong hybridization between them, as discussed earlier. The average value of the change in the valence electron number Δn is in the same order as the electronegativity, i.e., Zr (1.33), Ti (1.54), V (1.63), Mo (2.16), and C (2.55).

We find that the MH long-range order has a considerable effect on the charge transfer of $(TiVZrMo)_2C$ HE MXenes. Taking Zr as an example, Δn (1.145) in the MH structure is larger than that (1.100) in the random structure. The local clustering of Zr in the random structure leads to a local atomic environment composed of Zr and C atoms. However, in the MH structure, the MH long-range order suppresses local clustering, resulting in the presence of other transition metals in the neighboring sites of Zr. Consequently, Zr atoms, having the lowest electronegativity, tend to lose extra valence electrons, which are then transferred to neighboring transition metal atoms of other types. Similarly, charge transfer in other transition metals can be understood in the same way. In addition, we quantify the fluctuation of valence states with the standard deviation σ of the number of valence electrons in different atoms of the same element. Notably, σ in the random structure is larger than that in the MH structure. The suppressed fluctuation of valence states in the MH structure can once again be attributed to the MH long-range order compared to the random structure since the suppressed local clustering of the same atomic species leads to a more stable local atomic environment.

TABLE II. The Bader charge analysis of representative MH and random structures of $(TiVZrMo)_2C$ HE MXenes. Δn represents the average value of the change in the valence electron number, and σ represents the standard deviation of the number of valence electrons in different atoms of the same element.

	MH		Random	
Elements	Δn	σ	Δn	σ
Ti	1.097	0.020	1.090	0.039
V	0.777	0.022	0.797	0.047
Zr	1.145	0.029	1.100	0.062
Mo	0.322	0.031	0.380	0.072
C	−1.671	0.064	−1.684	0.103

In summary, we presented a novel MH model for HE MXenes and exemplified it through the $(TiVZrMo)_2C$ HE MXene. Due to the hidden long-range order, the MH model leads to lower energy and smaller deviation from Vegard's law compared to the prevailing (quasi)random models of the HE MXenes. The results align with our analysis of the elemental mapping images[36] obtained from the high-angle annular dark-field scanning transmission electron microscopy combined with X-ray energy dispersive spectroscopy, showing that transition metal atoms tend to distribute hyperuniformly. Additionally, the MH structure exhibits a distinctly smaller lattice distortion, which has a vital effect on the electronic properties of HE MXenes such as DOS and charge distribution. Previous experimental research suggested that the strong strains in the HE MXene atomic layers are beneficial for the nucleation and growth of lithium in lithium-ion battery applications.[75] These findings imply that our MH model may account for some of the major discrepancies. For example, the practical lithium storage capacity of MXenes falls short of its theoretical value.

It is also important to explore the electrochemical properties of HE MXenes and their potential in energy storage applications. However, the complexity of the surface environment leads to abundant adsorption sites for ions such as lithium and zinc. Due to the MH long-range order, large-scale systems for HE MXenes cause an extremely high computational cost for DFT calculations. In future work, we plan to develop machine-learning potentials. Capitalizing on its low computational overhead, the machine-learning potential enables us to perform an extensive investigation to assess the impact of multihyperuniformity on the lithium storage capacity of MXenes.

See the supplementary material for the procedure of image processing, multi-scale packing algorithm, DFT computational details, and supporting data.

Y.L. and M.C. are supported by the National Natural Science Foundation of China under Grant Nos. 12122401, 12074007, and 12135002. The numerical simulations were performed on the High Performance Computing Platform of CAPT.

AUTHOR DECLARATIONS

Conflict of Interest

The authors have no conflicts to disclose.

Author Contributions

Yu Liu: Conceptualization (lead); Data curation (lead); Formal analysis (lead); Investigation (lead); Methodology (lead); Project administration (equal); Software (equal); Validation (lead); Visualization (lead); Writing – original draft (lead); Writing – review & editing (lead). **Mohan Chen:** Funding acquisition (lead); Project administration (equal); Resources (lead); Software (lead); Supervision (lead); Writing – original draft (supporting); Writing – review & editing (equal).

DATA AVAILABILITY

The data that support the findings of this study are available from the corresponding author upon reasonable request.

REFERENCES

[1]M. Naguib, M. Kurtoglu, V. Presser, J. Lu, J. Niu, M. Heon, L. Hultman, Y. Gogotsi, and M. W. Barsoum, Adv. Mater. **23**, 4248 (2011).
[2]M. Naguib, O. Mashtalir, J. Carle, V. Presser, J. Lu, L. Hultman, Y. Gogotsi, and M. W. Barsoum, ACS Nano **6**, 1322 (2012).
[3]M. W. Barsoum and M. Radovic, Annu. Rev. Mater. Res. **41**, 195 (2011).
[4]M. Sokol, V. Natu, S. Kota, and M. W. Barsoum, Trends Chem. **1**, 210 (2019).
[5]S. A. Mirkhani, A. Shayesteh Zeraati, E. Aliabadian, M. Naguib, and U. Sundararaj, ACS Appl. Mater. Interfaces **11**, 18599 (2019).
[6]M. R. Lukatskaya, S. Kota, Z. Lin, M.-Q. Zhao, N. Shpigel, M. D. Levi, J. Halim, P.-L. Taberna, M. W. Barsoum, P. Simon *et al.*, "Ultra-high-rate pseudocapacitive energy storage in two-dimensional transition metal carbides," *MXenes* (Jenny Stanford Publishing, 2023), pp. 723–743.
[7]A. Lipatov, H. Lu, M. Alhabeb, B. Anasori, A. Gruverman, Y. Gogotsi, and A. Sinitskii, Sci. Adv. **4**, eaat0491 (2018).
[8]V. Kamysbayev, A. S. Filatov, H. Hu, X. Rui, F. Lagunas, D. Wang, R. F. Klie, and D. V. Talapin, Science **369**, 979 (2020).
[9]C. Chen, X. Xie, B. Anasori, A. Sarycheva, T. Makaryan, M. Zhao, P. Urbankowski, L. Miao, J. Jiang, and Y. Gogotsi, Angew. Chem., Int. Ed. **57**, 1846 (2018).
[10]C. Zhang, S.-H. Park, A. Seral-Ascaso, S. Barwich, N. McEvoy, C. S. Boland, J. N. Coleman, Y. Gogotsi, and V. Nicolosi, Nat. Commun. **10**, 849 (2019).
[11]X. Li, N. Li, Z. Huang, Z. Chen, G. Liang, Q. Yang, M. Li, Y. Zhao, L. Ma, B. Dong *et al.*, Adv. Mater. **33**, 2006897 (2021).
[12]Q. Meng, J. Ma, Y. Zhang, Z. Li, C. Zhi, A. Hu, and J. Fan, Nanoscale **10**, 3385 (2018).
[13]Q. Meng, J. Ma, Y. Zhang, Z. Li, A. Hu, J.-J. Kai, and J. Fan, J. Mater. Chem. A **6**, 13652 (2018).
[14]N. Li, Q. Meng, X. Zhu, Z. Li, J. Ma, C. Huang, J. Song, and J. Fan, Nanoscale **11**, 8485 (2019).
[15]X. Li, N. Li, Z. Huang, Z. Chen, Y. Zhao, G. Liang, Q. Yang, M. Li, Q. Huang, B. Dong *et al.*, ACS Nano **15**, 1718 (2021).
[16]F. Shahzad, M. Alhabeb, C. B. Hatter, B. Anasori, S. Man Hong, C. M. Koo, and Y. Gogotsi, Science **353**, 1137 (2016).
[17]M. Han, C. E. Shuck, R. Rakhmanov, D. Parchment, B. Anasori, C. M. Koo, G. Friedman, and Y. Gogotsi, ACS Nano **14**, 5008 (2020).
[18]Z. Lv, W. Ma, M. Wang, J. Dang, K. Jian, D. Liu, and D. Huang, Adv. Funct. Mater. **31**, 2102576 (2021).
[19]J. Li, C. Hou, C. Chen, W. Ma, Q. Li, L. Hu, X. Lv, and J. Dang, ACS Nano **17**, 10947 (2023).
[20]Y. Guo, T. Wang, Q. Yang, X. Li, H. Li, Y. Wang, T. Jiao, Z. Huang, B. Dong, W. Zhang *et al.*, ACS Nano **14**, 9089 (2020).
[21]Y. Xia, T. S. Mathis, M.-Q. Zhao, B. Anasori, A. Dang, Z. Zhou, H. Cho, Y. Gogotsi, and S. Yang, Nature **557**, 409 (2018).
[22]W. Ma, M. Wang, Q. Yi, D. Huang, J. Dang, Z. Lv, X. Lv, and S. Zhang, Nano Energy **96**, 107129 (2022).
[23]J.-W. Yeh, S.-K. Chen, S.-J. Lin, J.-Y. Gan, T.-S. Chin, T.-T. Shun, C.-H. Tsau, and S.-Y. Chang, Adv. Eng. Mater. **6**, 299 (2004).
[24]B. Cantor, I. T. H. Chang, P. Knight, and A. J. B. Vincent, Mater. Sci. Eng.: A **375**, 213 (2004).
[25]A. Sarkar, Q. Wang, A. Schiele, M. R. Chellali, S. S. Bhattacharya, D. Wang, T. Brezesinski, H. Hahn, L. Velasco, and B. Breitung, Adv. Mater. **31**, 1806236 (2019).
[26]E. P. George, W. A. Curtin, and C. C. Tasan, Acta Mater. **188**, 435 (2020).
[27]X. Wang, Q. Dong, H. Qiao, Z. Huang, M. T. Saray, G. Zhong, Z. Lin, M. Cui, A. Brozena, M. Hong *et al.*, Adv. Mater. **32**, 2002853 (2020).
[28]M. Cui, C. Yang, B. Li, Q. Dong, M. Wu, S. Hwang, H. Xie, X. Wang, G. Wang, and L. Hu, Adv. Energy Mater. **11**, 2002887 (2021).
[29]S. K. Nemani, B. Zhang, B. C. Wyatt, Z. D. Hood, S. Manna, R. Khaledialidusti, W. Hong, M. G. Sternberg, S. K. Sankaranarayanan, and B. Anasori, ACS Nano **15**, 12815 (2021).
[30]Z. Du, C. Wu, Y. Chen, Q. Zhu, Y. Cui, H. Wang, Y. Zhang, X. Chen, J. Shang, B. Li *et al.*, Adv. Energy Mater. **12**, 2103228 (2022).
[31]W. Ma, Z. Qiu, J. Li, L. Hu, Q. Li, X. Lv, and J. Dang, J. Energy Chem. **85**, 301 (2023).
[32]C. Tan, W. Ma, L. Hu, Q. Li, X. Lv, and J. Dang, Acta Mater. **267**, 119713 (2024).
[33]H. W. Seong, M. S. Lee, and H. J. Ryu, J. Mater. Chem. A **11**, 5681 (2023).
[34]A. Zunger, S.-H. Wei, L. G. Ferreira, and J. E. Bernard, Phys. Rev. Lett. **65**, 353 (1990).
[35]A. Van de Walle, P. Tiwary, M. De Jong, D. Olmsted, M. Asta, A. Dick, D. Shin, Y. Wang, L.-Q. Chen, and Z.-K. Liu, Calphad **42**, 13 (2013).
[36]X. He, Y. Qian, C. Wu, J. Feng, X. Sun, Q. Zheng, X. Li, and J. Shen, Adv. Mater. **35**, 2211432 (2023).
[37]W. Ma, Z. Qiu, M. Wang, C. Tan, L. Hu, X. Lv, Q. Li, J. Li, and J. Dang, Scr. Mater. **235**, 115596 (2023).
[38]S. Torquato and F. H. Stillinger, Phys. Rev. E **68**, 041113 (2003).
[39]S. Torquato, Phys. Rep. **745**, 1 (2018).
[40]M. Florescu, S. Torquato, and P. J. Steinhardt, Proc. Natl. Acad. Sci. U S A. **106**, 20658 (2009).
[41]W. Man, M. Florescu, E. P. Williamson, Y. He, S. R. Hashemizad, B. Y. Leung, D. R. Liner, S. Torquato, P. M. Chaikin, and P. J. Steinhardt, Proc. Natl. Acad. Sci. U S A. **110**, 15886 (2013).
[42]Y. Jiao, T. Lau, H. Hatzikirou, M. Meyer-Hermann, J. C. Corbo, and S. Torquato, Phys. Rev. E **89**, 022721 (2014).
[43]D. Hexner and D. Levine, Phys. Rev. Lett **114**, 110602 (2015).
[44]R. L. Jack, I. R. Thompson, and P. Sollich, Phys. Rev. Lett. **114**, 060601 (2015).
[45]Y. Xu, S. Chen, P.-E. Chen, W. Xu, and Y. Jiao, Phys. Rev. E **96**, 043301 (2017).
[46]D. Chen and S. Torquato, Acta Mater. **142**, 152 (2018).
[47]A. Chremos and J. F. Douglas, Phys. Rev. Lett. **121**, 258002 (2018).
[48]M. A. Klatt, J. Lovrić, D. Chen, S. C. Kapfer, F. M. Schaller, P. W. Schönhöfer, B. S. Gardiner, A.-S. Smith, G. E. Schröder-Turk, and S. Torquato, Nat. Commun. **10**, 811 (2019).
[49]Q.-L. Lei and R. Ni, Proc. Natl. Acad. Sci. U S A. **116**, 22983 (2019).
[50]Q.-L. Lei, M. P. Ciamarra, and R. Ni, Sci. Adv. **5**, eaau7423 (2019).
[51]Y. Zheng, L. Liu, H. Nan, Z.-X. Shen, G. Zhang, D. Chen, L. He, W. Xu, M. Chen, Y. Jiao *et al.*, Sci. Adv. **6**, eaba0826 (2020).
[52]M. Huang, W. Hu, S. Yang, Q.-X. Liu, and H. Zhang, Proc. Natl. Acad. Sci. U. S. A. **118**, e2100493118 (2021).
[53]D. Chen, Y. Zheng, L. Liu, G. Zhang, M. Chen, Y. Jiao, and H. Zhuang, Proc. Natl. Acad. Sci. U. S. A. **118**, e2016862118 (2021).
[54]M. A. Klatt, P. J. Steinhardt, and S. Torquato, Phys. Rev. Lett. **127**, 037401 (2021).
[55]Y. Zheng, D. Chen, L. Liu, Y. Liu, M. Chen, H. Zhuang, and Y. Jiao, Phys. Rev. B **103**, 245413 (2021).
[56]Y. Jiao, Physica A **585**, 126435 (2022).
[57]D. Chen, Y. Liu, Y. Zheng, H. Zhuang, M. Chen, and Y. Jiao, Phys. Rev. B **106**, 235427 (2022).
[58]D. Chen, Y. Zheng, and Y. Jiao, Phys. Rev. B **104**, 174101 (2021).
[59]D. Chen, H. Zhuang, M. Chen, P. Y. Huang, V. Vlcek, and Y. Jiao, Appl. Phys. Rev. **10**, 021310 (2023).
[60]Y. Liu, D. Chen, J. Tian, W. Xu, and Y. Jiao, Phys. Rev. Lett. **133**, 028401 (2024).
[61]H. Zhuang, D. Chen, L. Liu, D. Keeney, G. Zhang, and Y. Jiao, J. Phys.: Condens. Matter **36**, 285703 (2024).
[62]S. Mkhonta, Z.-F. Huang, and K. Elder, arXiv:2409.12090 (2024).
[63]X. Bai, P. Hu, A. Li, Y. Zhang, A. Li, G. Zhang, Y. Xue, T. Jiang, Z. Wang, H. Cui *et al.*, Nature **634**, 80–84 (2024).
[64]D. Chen, X. Jiang, D. Wang, J. I. Vidallon, H. Zhuang, and Y. Jiao, Acta Mater. **246**, 118678 (2023).
[65]L. Vegard, Z. Phys. **5**, 17 (1921).
[66]Y. Jiao, H. Berman, T.-R. Kiehl, and S. Torquato, PLoS One **6**(11), 1–9 (2011).
[67]Y. Zou, H. Ma, and R. Spolenak, Nat. Commun. **6**, 7748 (2015).
[68]P. Hohenberg and W. Kohn, Phys. Rev. **136**, B864 (1964).
[69]W. Kohn and L. J. Sham, Phys. Rev. **140**, A1133 (1965).
[70]M. Chen, G. C. Guo, and L. He, J. Phys. Condens. Matter **22**, 445501 (2010).
[71]P. Li, X. Liu, M. Chen, P. Lin, X. Ren, L. Lin, C. Yang, and L. He, Comput. Mater. Sci. **112**, 503 (2016).

[72]Y. Liu, X. Liu, and M. Chen, J. Nucl. Mater. **545**, 152733 (2021).
[73]Y. Liu, X. Ding, M. Chen, and S. Xu, Phys. Chem. Chem. Phys. **24**, 15511 (2022).
[74]Y. Liu, Y. Zhang, N. Xiao, X. Li, F.-Z. Dai, and M. Chen, Acta Mater. **279**, 120294 (2024).
[75]Z. Du, C. Wu, Y. Chen, Z. Cao, R. Hu, Y. Zhang, J. Gu, Y. Cui, H. Chen, Y. Shi *et al.*, Adv. Mater. **33**, 2101473 (2021).
[76]G. Gui, J. Li, and J. Zhong, Phys. Rev. B **78**, 075435 (2008).
[77]M. Yankowitz, J. Jung, E. Laksono, N. Leconte, B. L. Chittari, K. Watanabe, T. Taniguchi, S. Adam, D. Graf, and C. R. Dean, Nature **557**, 404 (2018).
[78]G. Henkelman, A. Arnaldsson, and H. Jónsson, Comput. Mater. Sci. **36**, 354 (2006).
[79]E. Sanville, S. D. Kenny, R. Smith, and G. Henkelman, J. Comput. Chem. **28**, 899 (2007).
[80]W. Tang, E. Sanville, and G. Henkelman, J. Phys.: Condens. Matter **21**, 084204 (2009).